

# Flat-band plasmons in twisted bilayer transition metal dichalcogenides: twist angle, relaxation and band cutoff effects

Xueheng Kuang,<sup>1,2</sup> Zhen Zhan,<sup>1,\*</sup> and Shengjun Yuan<sup>1,†</sup>

<sup>1</sup>*Key Laboratory of Artificial Micro- and Nano-structures of Ministry of Education and School of Physics and Technology, Wuhan University, Wuhan 430072, China*

<sup>2</sup>*Imdea Nanoscience, Faraday 9, 28015 Madrid, Spain*

(Dated: October 26, 2021)

Twisted bilayer transition metal dichalcogenides are ideal platforms to study flat-band phenomena. In this paper, we investigate flat-band plasmons in doped twisted bilayer MoS<sub>2</sub> by employing a full tight-binding model and the random phase approximation. Twist-angle effects on flat-band plasmons in twisted bilayer MoS<sub>2</sub> show that plasmons at a smaller angle exhibit lower energy due to a flatter band, which is similar to the twisted bilayer graphene case. Besides, effects of band cutoff and doping on plasmons are studied. We find that, in relaxed samples, low-damped and quasi-flat plasmons emerge only in one-band calculation where merely intraband transitions in the doped flat band are considered, whereas classical plasmons of two dimensional electron gas emerge in multi-band calculations. In rigid samples that possess isolated flat bands, classical and quasi-flat plasmons appear in both slightly-doped and highly-doped cases. So one-band calculation is only accurate in system with isolated flat bands. Especially, isolation of the flat band from its adjacent bands is essential to observe a low-damped and quasi-flat plasmon mode. On the contrary, for relaxed samples, contribution of interband transitions between flat band and other bands to plasmons makes a significant influence in transforming plasmons dispersion and energy. We hope that our study on flat-band plasmons can be instructive for studying other twisted systems with flat bands.

## I. INTRODUCTION

Twisted bilayer graphene (TBG) with flat bands has opened an avenue to explore an abundant phenomena, for instance, localized and correlated states<sup>1-3</sup>, unconventional superconductivity<sup>4,5</sup>, and electronic collective excitations<sup>6-8</sup>. Intrinsically undamped plasmons are discovered in TBG<sup>7,8</sup>, which give insight into the unconventional superconductivity<sup>9-11</sup> and linear resistivity observed in experiment<sup>12</sup>. Recently, ultraflat bands are detected in twisted bilayer transition metal dichalcogenides (tb-TMDs) with a wide range of angles<sup>13-18</sup>, which become ideal platforms to extensively investigate many-body states<sup>19-26</sup> and optical excitons<sup>27-29</sup>. One could wonder whether the flat-band tb-TMDs possess similar plasmon properties as the TBG. Up to now, plasmons, the quanta of electronic collective excitations, have not been investigated in tb-TMDs yet. Therefore, twisted bilayer MoS<sub>2</sub> (tb-MoS<sub>2</sub>) with flat bands as a representation of tb-TMDs will be chose to study its plasmons that are related to collective excitation behaviours of flat-band electrons.

In previous works, plasmons in two-dimensional (2D) TMDs without showing flat bands have been extensively studied within density functional theory<sup>30-39</sup>, effective low-energy model<sup>40-43</sup> and tight-binding model (TB)<sup>44</sup>. Plasmons with negative and  $\sqrt{q}$  dispersion are discovered in charge-density wave 2D-TMDs<sup>30-32,35,45-47</sup>, such as TaS<sub>2</sub>, NbSe<sub>2</sub> and TaSe<sub>2</sub>, where anisotropic plasmons can exist in 2H-TaS<sub>2</sub><sup>39</sup>. Besides, square root and linear plasmon (acoustic plasmon) modes are generated in

MoS<sub>2</sub><sup>36,40-43</sup>. Interactions between plasmon and quasi-particles, such as exciton and phonon, are also concerned in 2D-TMDs<sup>48-50</sup>. Currently, the study of plasmons in MoS<sub>2</sub> cover monolayer<sup>40-44,51</sup>, two-layer<sup>36</sup>, few-layer<sup>37,38</sup>, and one-sheet systems<sup>34,52</sup>, whereas systems with twist angles have not been studied yet. Thus, we are also motivated to complete the study of plasmons in 2D TMDs with a particular case, tb-MoS<sub>2</sub>.

Our previous work pointed out that flat-band TBG shows intrinsically low-damped and quasi-flat plasmon modes<sup>8</sup>. The tb-MoS<sub>2</sub> systems are semiconductor<sup>13,14</sup>. We need to dope tb-MoS<sub>2</sub> to investigate low-energy plasmons via a TB model and random phase approximation (RPA). Ultraflat bands can be observed in the valence band (VB) of tb-MoS<sub>2</sub> with a wide range of twist angles, and flat bands get narrower at a smaller angle<sup>13,16,53</sup>. By changing the twist angle of tb-MoS<sub>2</sub>, we can study how flatness of flat bands modify the collective excitations. Moreover, when consider the lattice relaxation, a band gap between flat band at the VB and other lower bands disappears. Will such absence of band gaps affect the plasmon? In principle, polarization functions can be calculated via the Lindhard function<sup>54</sup>. With this method, we can implement the band cutoff in our plasmon calculations. For instance, we can perform only one-band calculation by considering collective excitations in a single flat band, which is recognized as “flat-band plasmons” that defined in TBG<sup>7</sup>. A full-band calculation can also be realized via a combination of Kubo formula and tight-bind propagation method (TBPM)<sup>55,56</sup>. The effect of the band cutoff on the flat-band plasmon can be studied with these two methods. Furthermore, interband transition effects on plasmons are investigated by tuning bands cutoff and doping levels in relaxed samples. Our work could be an example to study flat-band plasmons in other twisted

\* Corresponding author: zhen.zhan@whu.edu.cn

† Corresponding author: s.yuan@whu.edu.cn

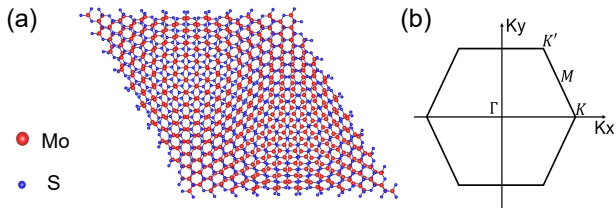


FIG. 1. (a) Top view of the atomic structure of  $3.5^\circ$  tb-MoS<sub>2</sub>. (b) The first BZ with high symmetry points for the hexagonal lattice of tb-MoS<sub>2</sub>.

2D semiconductors.

This paper is organized as following. In Sec. II, the tight-binding model and computational methods are introduced. In Sec. III, flat-band plasmons of relaxed samples with varied twist angles and of a rigid sample are studied in details. In Sec. IV, We pay attention to the effects of bands cutoff and chemical potentials on plasmons. Finally, we give a summary and discussion of our work.

## II. NUMERICAL METHODS

### II.1. Tight-binding model

We construct atomic structures of tb-MoS<sub>2</sub> with a commensurate approach used in building TBG structure<sup>57,58</sup>. The twisted structures have an initial 2H stacking bilayer and then rotate one layer with the origin at an atom site<sup>17</sup>. The atomic structure of a moiré pattern of tb-MoS<sub>2</sub> with  $\theta = 3.5^\circ$  is shown in Fig. 1(a), which contains 1626 atoms. In this paper, we mainly focus on plasmonic properties of tb-MoS<sub>2</sub> with  $\theta = 3.5^\circ$  and  $\theta = 5.1^\circ$ . The fully atomic relaxation can be simulated via LAMMPS package<sup>59</sup> with the intralayer Stilliner-Weber potential<sup>60</sup> and the interlayer potential Lennard-Jones potential<sup>61</sup>. The relaxation effects on flat bands of tb-MoS<sub>2</sub> are investigated in former works<sup>13,14</sup>.

Here, we employ an accurate multi-orbital tight-binding model to investigate electronic properties of tb-MoS<sub>2</sub>. In the tight-binding model, one unit cell of monolayer transition metal dichalcogenides comprises 11 orbitals, 5 d orbitals from one Mo atom and 6 p orbitals from two S atoms<sup>62</sup>. The total Hamiltonian of twisted bilayer MoS<sub>2</sub> can be written as

$$\hat{H} = \hat{H}_1^{(1L)} + \hat{H}_2^{(1L)} + \hat{H}_{int}^{(2L)}, \quad (1)$$

where  $\hat{H}_{1(2)}^{(1L)}$  is the eleven-orbital single layer Hamiltonian, which contains the on-site energy, the hopping terms between orbitals of the same type at first-neighbor positions and the hopping terms between orbitals of different type at first- and second-neighbor positions. The

term  $\hat{H}_{int}^{(2L)}$  is the interlayer interaction expressed as

$$\begin{aligned} \hat{H}_{int}^{2L} = & \sum_{p'_i, \mathbf{r}_2, p_j, \mathbf{r}_1} \hat{\phi}_{2, p'_i}^\dagger(\mathbf{r}_2) t_{p'_i, p_j}^{(LL)}(\mathbf{r}_2 - \mathbf{r}_1) \hat{\phi}_{1, p_j}(\mathbf{r}_1), \\ & + \text{H.c.}, \end{aligned} \quad (2)$$

where  $\hat{\phi}_{i, p_j}$  is the  $p_j$  orbital basis of  $i$ -th monolayer. The interlayer hoppings in Slater-Koster (SK) relation are expressed with distance and angle as<sup>63</sup>

$$t_{p'_i, p_j}^{(LL)}(\mathbf{r}) = (V_{pp, \sigma}(r) - V_{pp, \pi}(r)) \frac{r_i r_j}{r^2} + V_{pp, \pi}(r) \delta_{i, j}, \quad (3)$$

where  $r = |\mathbf{r}|$  and the distance-dependent SK parameter is

$$V_{pp, b} = \nu_b e^{[-(r/R_b)^{\eta_b}]}, \quad (4)$$

where  $b = \sigma, \pi$ ,  $\nu_b$ ,  $R_b$  and  $\eta_b$  are constant values taken from the Ref. 62. In this paper, the interlayer interactions in twisted bilayer MoS<sub>2</sub> are included in the TB Hamiltonian by adding hoppings between p orbitals of S atoms in top and bottom layers with distance smaller than 5 Å. Recent study shows that such first-neighbor interlayer hopping approximation is appropriate enough<sup>53</sup>. When we relax the system, atoms moves away from its equilibrium position in both in-plane and out-of-plane. As a consequence, we also need to change the intralayer hopping in Eq. (1). The intralayer hoppings in relaxed samples are modified with the form<sup>64</sup>

$$t_{ij, \mu\nu}^{intra}(\mathbf{r}_{ij}) = t_{ij, \mu\nu}^{intra}(\mathbf{r}_{ij}^0) \left( 1 - \Lambda_{ij, \mu\nu} \frac{|\mathbf{r}_{ij} - \mathbf{r}_{ij}^0|}{|\mathbf{r}_{ij}^0|} \right) \quad (5)$$

where  $t_{ij, \mu\nu}^{intra}$  is the intralayer hopping between the  $\mu$  orbital of the  $i$  atom and  $\nu$  orbital of the  $j$  atom,  $\mathbf{r}_{ij}^0$  and  $\mathbf{r}_{ij}$  are the distance between the  $i$  and  $j$  atoms in the equilibrium and relaxed cases,  $\Lambda_{ij, \mu\nu}$  is the dimensionless bond-resolved local electron-phonon coupling. We assume that  $\Lambda_{ij, \mu\nu} = 3, 4, 5$  for the S-S  $pp$ , S-Mo  $pd$  and Mo-Mo  $dd$  hybridizations, respectively<sup>64</sup>. Note that a large Hamiltonian matrix describing a rigid or relaxed tb-MoS<sub>2</sub> supercell will be generated. For example, the items in  $3.5^\circ$  MoS<sub>2</sub> Hamiltonian matrix exceed five thousand. Consequently, it is tough for one to do full-band calculations with such a large matrix. Next, we will introduce numerical methods for exploring plasmonic properties in doped tb-MoS<sub>2</sub>.

### II.2. Plasmon

Polarization functions of tb-MoS<sub>2</sub> with full-band calculations are performed by combining Kubo formula<sup>65</sup> with TBPM as<sup>56</sup>

$$\begin{aligned} \Pi_K(\mathbf{q}, \omega) = & -\frac{2}{S} \int_0^\infty dt e^{i\omega t} \text{Im} \langle \varphi | n_F(H) e^{iHt} \\ & \times \rho(\mathbf{q}) e^{-iHt} [1 - n_F(H)] \rho(-\mathbf{q}) | \varphi \rangle, \end{aligned} \quad (6)$$

where  $n_F(H) = \frac{1}{e^{\beta(H-\mu)} + 1}$  is the Fermi-Dirac distribution operator,  $\beta = \frac{1}{k_B T}$  with  $T$  being the temperature,

$k_B$  the Boltzmann constant and  $\mu$  the chemical potential.  $\rho(\mathbf{q}) = \sum_i c_i^\dagger c_i \exp(i\mathbf{q} \cdot \mathbf{r}_i)$  is the density operator and  $S$  is the area of a unit cell of tb-MoS<sub>2</sub>. The dynamical polarization function also can be obtained from the Lindhard function<sup>54</sup>

$$\begin{aligned} \Pi(\mathbf{q}, \omega) = & -\frac{g_s}{(2\pi)^2} \int_{\text{BZ}} d^2\mathbf{k} \sum_{l,l'} \frac{n_F(E_{\mathbf{k}l}) - n_F(E_{\mathbf{k}l'})}{E_{\mathbf{k}l} - E_{\mathbf{k}l'} + \hbar\omega + i\delta} \\ & \times |\langle \mathbf{k}'l' | e^{i\mathbf{q} \cdot \mathbf{r}} | \mathbf{k}l \rangle|^2, \end{aligned} \quad (7)$$

where  $|\mathbf{k}l\rangle$  and  $E_{\mathbf{k}l}$  are eigenstates and eigenvalues of the TB Hamiltonian in Eq. (1), respectively, with  $l$  and  $l'$  being band indices,  $\mathbf{k}' = \mathbf{k} + \mathbf{q}$ ,  $\delta \rightarrow 0^+$ . Generally, the integral is taken over the whole first Brillouin zone (BZ) shown in Fig. 1 (b). It is hard to sum over total bands obtained by diagonalizing TB Hamiltonian in Eq. (1) of a supercell that contains thousand of atoms. However, it is convenient for ones to analyze bands contribution to polarization functions as it can be written as the sum of two parts

$$\Pi(\mathbf{q}, \omega) = \Pi_{\text{intra}}(\mathbf{q}, \omega) + \Pi_{\text{inter}}(\mathbf{q}, \omega), \quad (8)$$

where  $\Pi_{\text{intra}}(\mathbf{q}, \omega)$  and  $\Pi_{\text{inter}}(\mathbf{q}, \omega)$  denote intraband and interband contributions corresponding to  $l = l'$  and  $l \neq l'$  in Eq. (7), respectively.

With the polarization function acquired from either Kubo formula in Eq. (6) or Lindhard function in Eq. (7), the dielectric function that describes the electronic response to extrinsic electric perturbation, can be written within RPA as

$$\varepsilon(\mathbf{q}, \omega) = 1 - V(q)\Pi(\mathbf{q}, \omega), \quad (9)$$

in which  $V(q) = 2\pi e^2 / (\varepsilon_B q)$  is the Fourier component of two-dimensional Coulomb interaction, with  $\varepsilon_B$  being the background dielectric constant. In our calculations, we set  $\varepsilon_B = 3.03$  to represent the dielectric constant of the hexagonal boron nitride (hBN). The energy loss function can be expressed as

$$S(\mathbf{q}, \omega) = -\text{Im}(1/\varepsilon(\mathbf{q}, \omega)), \quad (10)$$

which is an experimentally observable quantity to reflect the electronic response density.

### II.3. Density of states

The density of states (DOS) for tb-MoS<sub>2</sub> is calculated by using the TBPM<sup>55</sup> in frame of a full TB model. The TBPM method makes it possible to obtain the electronic properties of large-scale systems, for instance, the DOS of TBG with rotation angle  $\theta$  down to  $0.48^\circ$ <sup>66</sup> and of dodecagonal graphene quasicrystal<sup>67,68</sup>

$$D(E) = \frac{1}{2\pi N} \sum_{p=1}^N \int_{-\infty}^{\infty} e^{iEt} \langle \varphi_p(0) | e^{-iHt} | \varphi_p(0) \rangle dt, \quad (11)$$

where  $|\varphi_p(0)\rangle$  is an initial state with the random superposition of basis states at all sites  $N$ . In our calculations,

the accuracy of electronic properties can be guaranteed by utilizing a large enough system with more than 10 million atoms.

### III. FLAT-BAND PLASMONS IN RELAXED AND RIGID MOS<sub>2</sub>

In this section, we focus on flat-band plasmons in relaxed and rigid hole-doped tb-MoS<sub>2</sub>. A single flat valence band emerges at  $5.1^\circ$  and  $3.5^\circ$  near zero energy, as shown in Fig. 2 (d) and (h), respectively. Here, bandwidth of the flat band (energy difference between the  $\Gamma$  and K points of BZ) for  $3.5^\circ$  (5.9 meV) is much smaller than the one for  $5.1^\circ$  (16.2 meV). The electronic density of states related to the flat bands show large peaks, the van Hove singularities (VHS). The doping levels, -10.0 meV and -2.4 meV, cross the flat bands and VHS are shown in Fig. 2(d) and (h), respectively. We analyze the plasmonic properties in the loss function spectra and electron-hole continuum in Fig. 2. The first and second rows in Fig. 2 show the results for tb-MoS<sub>2</sub> with  $5.1^\circ$  and  $3.5^\circ$ , respectively. The results shown in Fig. 2(a), (b), (e) and (f) are obtained from the Lindhard function in Eq. (7) with band cutoff, whereas full-band calculations are performed via Kubo formula in Eq. (6) in Fig. 2(c) and (g). The spectra with notation ‘‘1b-cut’’ in Fig. 2(a) and (e) are calculated by only summing over the single doped flat band in Eq. (7), and the spectra with notation ‘‘20b-cut’’ in Fig. 2 (b) and (f) are obtained by summing over extra 40 bands near the flat band (20 bands above and 20 bands below the Fermi level) in Eq. (7).

When we merely sum over the flat band in Lindhard function, only intraband transitions are taken into account and the interband transitions from the doped flat band to other bands are omitted with the second term in Eq. (8) set as zero. In this case, plasmon modes appeared in  $5.1^\circ$  and  $3.5^\circ$  tb-MoS<sub>2</sub> are quasi-flat and low-damped, as they are located above the single-particle continuum. They can be recognized as the ‘‘flat-band plasmons’’<sup>7,8,69</sup>. Here, this kind of plasmon modes are governed simply by intraband transitions inside the flat band, which verify that flat bands can lead to flat plasmons in an extremely simplified model. Moreover, the plasmon with energy in Fig. 2(e) is lower than that in Fig. 2(a), which is mainly because of the decreased bandwidth of the flat band with a smaller twist angle.

From the band structure in Fig. 2(d) and (h), it is obvious that the doped flat bands are not completely isolated from other bands. In principle, we not only include the transitions within flat bands, but also consider effects of interband transitions on the flat-band plasmons. When extra 40 bands are included in the Lindhard function, classical plasmon modes occur with  $\sqrt{q}$  dispersion denoted by the fitted black lines in Fig. 2(b) and (f), which do not cross the continuum showing a low Landau-damping feature. Comparing the plasmon modes in Fig. 2(b) and (f) to those in Fig. 2(a) and (e), the effect of interband transitions on the doped flat-band plasmons are

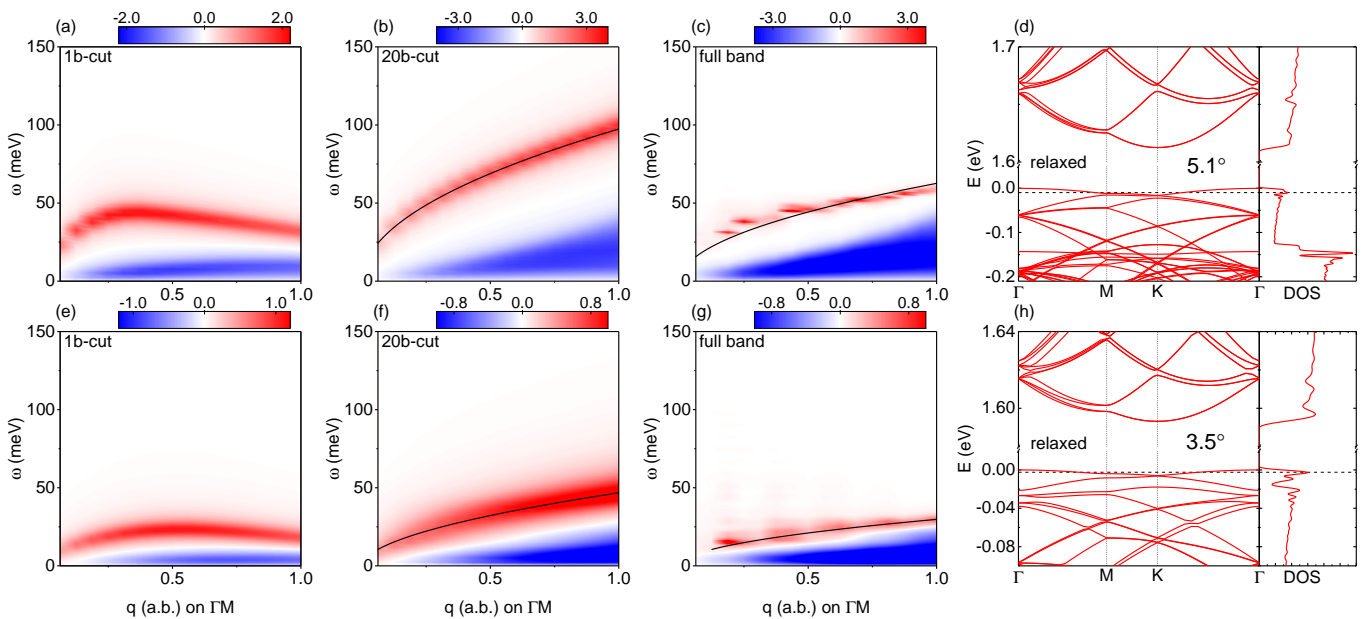


FIG. 2. The loss function density (positive) and single-particle continuum (negative) plots of relaxed tb-MoS<sub>2</sub> with 5.1° (a),(b) and (c) as well as 3.5° (e),(f) and (g) with different band cutoff calculations. Band structures and DOS for 5.1° (d) and 3.5° (h) are shown over a small energy range. The dashed lines crossing the flat bands in (d) and (h) denote the chemical potential  $\mu = -10.0$  meV and  $\mu = -2.4$  meV, respectively. Here, the Fermi energy zero is set as the valence band maximum (VBM). In (a) and (e), only single doped flat-band transitions are included with  $l = l' = 1$  in Eq. (7), while the flat band and 40 bands close to it (20 bands above and 20 bands below it) are summed in (b) and (f) calculation. Full-band calculations are performed via Eq. (6) in (c) and (g). The maximum value for  $q$  (a.b.) = 1 represents the length from  $\Gamma$  to M point denoted in Fig. 1 and temperature is 1 K.

significant. It changes the quasi-flat dispersion of plasmon modes into  $\sqrt{q}$  dispersion and dramatically enhances the energy of plasmons with larger  $q$ . In fact, previous work shows that interband transitions can also decrease plasmon energies in other TMD materials<sup>32,70</sup>.

We further investigate how interband transitions from higher energy bands to the doped flat band affect the plasmonic properties in Fig. 2(c) and (g), which is obtained from a full-band calculation including transitions among all bands via TBPM<sup>56</sup>. Classical plasmon modes of 2D electronic gas still exist in Fig. 2(c) and (g), but possess lower energy compared to the Fig. 2(b) and (f). It means that interband transitions beyond an energy range of the “20b-cut” screen those interband transitions among 40 bands at large  $q$ . The plasmon mode marked by a black line tends to be a linear dispersion, but it is not an acoustic mode with linear dispersion induced by oscillation of Fermi gases with different Fermi velocity within the flat band<sup>41,43,71</sup>. The energy distribution of single-particle continuum spectra in Fig. 2(c) and (g) are barely changed when compare to Fig. 2(b) and (f). Single-particle transitions in the low energy range (0 - 150 meV) have been completely covered by 40 bands, since the imaginary part of the polarization function in a specific energy range are not affected by higher energy bands located beyond the range. However, the real part of the polarization function in a specific energy range can be affected by those transitions beyond the energy range, resulting in a difference of low-energy plasmons in Fig.

2(b) and (c) or (f) and (g).

We have analyzed the plasmonic properties in above three band cutoffs. The quasi-flat plasmons only appear in one-band calculation, which are induced only by intra-band transitions in the doped flat band. After that, if we consider more bands, the plasmonic features are notably affected by interband transitions. The effects of multi-band transitions on the flat-band plasmon in tb-MoS<sub>2</sub> are different from that in TBG<sup>7</sup>. Here, quasi-flat plasmons in the simplified one-band calculation change to classical ones in multi-band and full-band calculations. However, for the TBG, classical plasmons in a two-band toy model are distinct from quasi-flat ones in the multi-band continuum model<sup>7</sup>, and the quasi-flat feature still reserves in a full TB calculation<sup>8</sup>. Moreover, the rigid TBG with flat band touch with other energy bands still possesses ultraflat plasmons<sup>72</sup>. The different band structure effects on flat-band plasmons of TBG and tb-MoS<sub>2</sub> might originate from different feature of the flat bands in the two twisted systems. The flat bands in relaxed magic-angle TBG are completely isolated from other bands with gaps at least two times larger than the bandwidth<sup>8</sup>, while the doped flat band in relaxed tb-MoS<sub>2</sub> only isolates from those bands above zero energy but touch with the negative energy band at K point, as shown in Fig. 2 (d) and (h).

In order to further unveil reasons resulting in such significant difference, we study the flat-band plasmons in rigid tb-MoS<sub>2</sub> with 3.5° in Fig. 3. The single flat

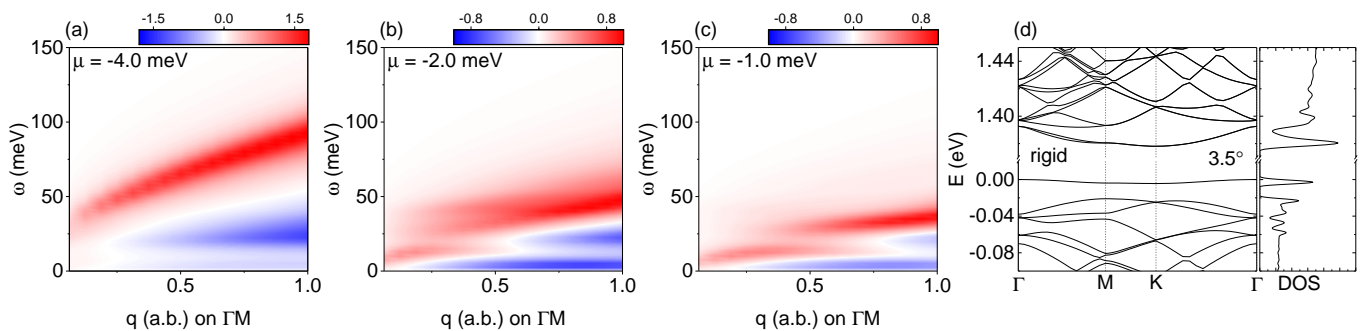


FIG. 3. The loss function and single-particle continuum density plots for rigid  $3.5^\circ$  twisted bilayer MoS<sub>2</sub> with chemical potential (a)  $\mu = -4.0$  meV, (b)  $\mu = 2.0$  meV and (c)  $\mu = -1.0$  meV, with “20b-cut” calculation. Temperature is 1 K. Band structure and DOS are plotted in (d) for rigid  $3.5^\circ$  MoS<sub>2</sub>.

band with bandwidth 4.3 meV is completely isolated from other bands as shown in Fig. 3 (d). The gap (15.8 meV) between the flat band and the band with negative energy at M point is three times larger than the bandwidth. The plasmon spectra are obtained by a “20b-cut” calculation and shown in Fig. 3(a), (b) and (c) with different chemical potentials, -4.0 meV, -2.0 meV and -1.0 meV, respectively. In the highly doped case in Fig. 3(a), only a classical 2D plasmon mode emerges, whereas the low-energy quasi-flat plasmon modes re-appear and extra interband modes also appear when doping level at -2.0 meV and -1.0 meV in Fig. 3(b) and (c).

Here, different chemical potentials can tune the intraband and interband contributions to the total polarization function in Eq. (8). The interband transitions dominate the total loss function in the deep-doping case, so that the quasi-flat plasmons vanish because the flat plasmons are mainly originated from the intraband transitions in the doped flat band. In Fig. 3(a), the intensity of single-particle continuum below 10 meV is relatively lighter, implying weaker intraband transitions of flat band. However, in the lower doping cases where the doping levels -2.0 meV and -1.0 meV are close to the energy of VHS peak of the flat band, the intraband contributions to the polarization function are augmented in the low energy range (0 - 4.3 meV) as shown in single-particle continuum in Fig. 3(b) and (c). Interband transitions only occur at energies larger than 15.8 meV due to the existence of a band gap. The continuum spectra in Fig. 3(b) and (c) also split into two parts due to the band gap. Therefore, the quasi-flat intraband plasmon modes with lower energy can coexist with the interband ones with higher energy. The quasi-flat plasmon modes are low-damped as they reside at the gap between two parts of continuum spectra at small  $q$  and will be damped with  $q$  getting larger.

In brief, flat bands can lead to quasi-flat and low-damped plasmons in rigid tb-MoS<sub>2</sub>. In relaxed case, due to disappearance of the band gap between the flat band and its adjacent band, interband transitions can be induced in a very small energy range, which also allows the exist of intraband transitions. In the rigid sample, it is still critical to tune intraband and interband transitions

of the flat band for obtaining quasi-flat plasmon mode in tb-MoS<sub>2</sub> by decreasing doping levels. Here, tuning chemical potentials in relaxed samples fails to change the plasmon dispersion in our multi-band calculations as the interband transitions always interference with intraband transitions. But one could look forward to discover quasi-flat plasmons in other relaxed tb-TMDs, such as twisted bilayer MoSe<sub>2</sub>, which show isolated flat bands<sup>53,73</sup>.

#### IV. BAND CUTOFF AND DOPING EFFECT

In this part, we further investigate the different band cutoff and doping effects on plasmons in relaxed tb-MoS<sub>2</sub> with  $5.1^\circ$  and  $3.5^\circ$  in Fig. 4. We compare the plasmons calculated with different band cutoff in Fig. 4(a) and (c). Contributions from interband transitions to the plasmons can be tuned by changing the number of bands summed in Eq. (7). The plasmonic energy changes with wave number  $q$  at both  $5.1^\circ$  and  $3.5^\circ$ . The plasmonic energy significantly increases from one band calculation (black squares) to “20b-cut” calculation (red dots) with  $q$  getting larger. Then, after taking more bands (blue and green triangles) into account, the plasmonic energy decreases when  $q$  larger than 0.25 in Fig. 4(a) and  $q$  over 0.56 in Fig. 4(c). Note that the plasmonic energy window shown in Fig. 4 has been included in the energy range to allow all potential interband transitions in “20b-cut” calculation. Other interband transitions beyond the plasmonic energy window in “40b-cut” calculation and “80b-cut” calculation give rise to a redshift of plasmon energy for some large  $q$ . The plasmonic energy obtained from “20b-cut” calculation has been converged with that calculated with “40b-cut” and “160b-cut” calculations for  $q < 0.25$  in Fig. 4(a) and  $q < 0.56$  in Fig. 4(c). Thus, only for some small wave numbers, it is safe to model the low-energy plasmon with an appropriate bands cutoff calculation. Our bands cutoff calculation can be related to those performed in the frame of an effective low energy model that only considers specific number of electronic bands. Thus, one should be careful to use developed effective models to investigate plasmons in tb-TMD<sup>21,74,75</sup>.

When chemical potential is fixed, the contributions of

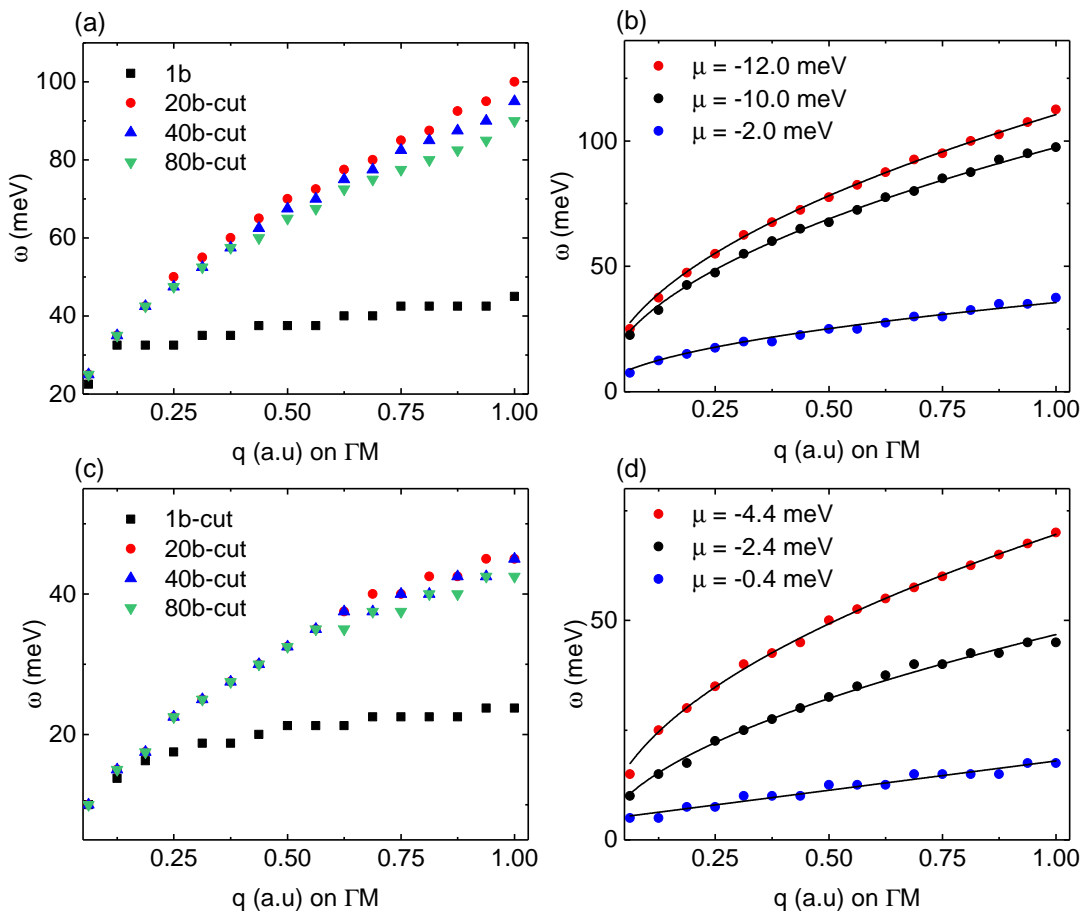


FIG. 4. Plasmon energy versus  $q$  for relaxed twisted bilayer  $\text{MoS}_2$  at  $5.1^\circ$  (a),(b) and  $3.5^\circ$  (c),(d). 1b (black square), 20b-cut (red circle), 40b-cut (blue triangle) and 80b-cut (green triangle) in (a) and (c) signify the 1 band (the doped flat band), 40 bands (20 bands above and 20 below the doped flat band), 80 bands (40 bands above and 40 below the doped flat band), and 160 bands (80 bands above and 80 below the doped flat band) cutoff calculations via Eq. (7) with  $l$  and  $l'$  summing over 1 band, 40 bands, 80 bands and 160 bands, respectively. Plasmon energy changes with three different chemical potentials in (b) and (d) with 20b-cut calculations via Eq. (7).

interband transitions can be tuned by considering different number of bands near the flat band. Besides, tuning chemical potentials is another method to vary contributions of interband and intraband transitions. In Fig. 4(b) at  $5.1^\circ$  and (d) at  $3.5^\circ$ , the plasmon curves are calculated in “20b-cut” situation. On the one hand, decreasing the chemical potential leads to smaller plasmonic energy at a particular  $q$ . Plasmonic energy dispersions keep the relation, square root of  $q$ , with different coefficients, as fitted by the black lines in Fig. 4(b) and (d). When doping levels get deeper, more electrons can participate in the higher-energy interband transitions that can contribute to higher plasmonic energy. The plasmonic energy dispersion tends to linear-like relation with  $q$  when doping level close to zero, as shown in the Fig. 4 (b) and (d) with blue dots. In this case, intraband transitions mainly occupy and Fermi velocity gets smaller as the flat band gets flatter when close to the  $\Gamma$  point. However, the plasmon mode with quasi-flat shape has not been observed in both high and low doping levels in relaxed  $\text{tb-MoS}_2$  with  $3.5^\circ$ . Thus, the separation of flat band from other bands in

$\text{tb-MoS}_2$  plays a crucial role in exploring the quasi-flat and low-damped plasmon modes.

## V. SUMMARY AND DISCUSSION

In summary, we investigated flat-band plasmons in doped  $\text{tb-MoS}_2$  with and without relaxation. In calculating the polarization function, different bands cut-off are employed to tune interband transitions between the single flat band to other bands. In relaxed cases, the single flat band are not separated from those bands blow it so that the interband and intraband transitions in the flat band can occur simultaneously over an extremely small energy range. When interband transitions interfere with intraband transitions in multi-band calculations, the quasi-flat plasmons emerging in the one-band calculation are transformed into classical plasmons of 2D electron gas with a square root of dispersion. The full band calculations including higher-energy interband transitions decrease plasmonic energies of classical plas-

mons. We also compared flat-band plasmons in relaxed tb-MoS<sub>2</sub> at 5.1° to those at 3.5°. The plasmonic energy gets smaller in all calculations when the twist angle decreases, since a smaller angle gives rise to a flatter band. In rigid case at 3.5°, the single flat band is isolated from other bands below it with a gap three times larger than its bandwidth. Interband transitions are independent of intraband ones because intraband transitions only occur below the energy of flat-band bandwidth while gap energy much larger than the bandwidth is needed to allow interband transitions. Therefore, quasi-flat intraband plasmons can survive with interband ones at low doping. Besides, different bands cutoff in multi-band calculations can change the plasmonic energy at large q. Changing chemical potentials in doped and relaxed tb-MoS<sub>2</sub> can tune plasmonic energy but fail to transform the plasmon shape to a quasi-flat one. All these behaviours are different from the TBG case.

In future, flat band systems are still potential platforms chasing low-damped and flat plasmons and their

applications. Based on the analysis of bands cutoff calculation, we also need to think about the validity of low-energy models in studying plasmons in flat-band systems, such as twisted bilayer materials with flat band touch with its adjacent bands.

## ACKNOWLEDGMENTS

We thank F. Guinea for his useful discussions. This work was supported by the National Natural Science Foundation of China (Grants No. 11774269 and No. 12047543). S.Y. acknowledges funding from the National Key R&D Program of China (Grant No. 2018YFA0305800). X.K. acknowledges the financial support from China Scholarship Council (CSC). Numerical calculations presented in this paper have been performed on the supercomputing system in the Supercomputing Center of Wuhan University.

- 
- <sup>1</sup> R. Bistritzer and A. H. MacDonald, Proceedings of the National Academy of Sciences **108**, 12233 (2011).
  - <sup>2</sup> Y. Cao, V. Fatemi, A. Demir, S. Fang, S. L. Tomarken, J. Y. Luo, J. D. Sanchez-Yamagishi, K. Watanabe, T. Taniguchi, E. Kaxiras, *et al.*, Nature **556**, 80 (2018).
  - <sup>3</sup> A. Kerelsky, L. J. McGilly, D. M. Kennes, L. Xian, M. Yankowitz, S. Chen, K. Watanabe, T. Taniguchi, J. Hone, C. Dean, *et al.*, Nature **572**, 95 (2019).
  - <sup>4</sup> Y. Cao, V. Fatemi, S. Fang, K. Watanabe, T. Taniguchi, E. Kaxiras, and P. Jarillo-Herrero, Nature **556**, 43 (2018).
  - <sup>5</sup> M. Yankowitz, S. Chen, H. Polshyn, Y. Zhang, K. Watanabe, T. Taniguchi, D. Graf, A. F. Young, and C. R. Dean, Science **363**, 1059 (2019).
  - <sup>6</sup> N. C. Hesp, I. Torre, D. Rodan-Legrain, P. Novelli, Y. Cao, S. Carr, S. Fang, P. Stepanov, D. Barcons-Ruiz, H. Herzig Sheinfux, *et al.*, Nature Physics **17**, 1162 (2021).
  - <sup>7</sup> C. Lewandowski and L. Levitov, Proceedings of the National Academy of Sciences **116**, 20869 (2019).
  - <sup>8</sup> X. Kuang, Z. Zhan, and S. Yuan, Physical Review B **103**, 115431 (2021).
  - <sup>9</sup> G. Sharma, M. Trushin, O. P. Sushkov, G. Vignale, and S. Adam, Physical Review Research **2**, 022040 (2020).
  - <sup>10</sup> C. Lewandowski, D. Chowdhury, and J. Ruhman, Physical Review B **103**, 235401 (2021).
  - <sup>11</sup> T. Cea and F. Guinea, Proceedings of the National Academy of Sciences **118**, e2107874118 (2021).
  - <sup>12</sup> J. González and T. Stauber, Physical Review Letters **124**, 186801 (2020).
  - <sup>13</sup> M. H. Naik and M. Jain, Physical Review Letters **121**, 266401 (2018).
  - <sup>14</sup> Z. Zhan, Y. Zhang, P. Lv, H. Zhong, G. Yu, F. Guinea, J. Á. Silva-Guillén, and S. Yuan, Physical Review B **102**, 241106 (2020).
  - <sup>15</sup> M. I. B. Utama, R. J. Koch, K. Lee, N. Leconte, H. Li, S. Zhao, L. Jiang, J. Zhu, K. Watanabe, T. Taniguchi, *et al.*, Nature Physics **17**, 184 (2021).
  - <sup>16</sup> V. Vitale, K. Atalar, A. A. Mostofi, and J. Lischner, 2D Materials **8**, 045010 (2021).
  - <sup>17</sup> Y. Zhang, Z. Zhan, F. Guinea, J. Á. Silva-Guillén, and S. Yuan, Physical Review B **102**, 235418 (2020).
  - <sup>18</sup> S. Kundu, M. H. Naik, H. Krishnamurthy, and M. Jain, arXiv preprint arXiv:2103.07447 (2021).
  - <sup>19</sup> H. Pan, F. Wu, and S. Das Sarma, Physical Review Research **2**, 33087 (2020).
  - <sup>20</sup> J. Zang, J. Wang, J. Cano, and A. J. Millis, Phys. Rev. B **104**, 075150 (2021).
  - <sup>21</sup> Y. Zhang, T. Liu, and L. Fu, Physical Review B **103**, 155142 (2021).
  - <sup>22</sup> L. Xian, M. Claassen, D. Kiese, M. M. Scherer, S. Trebst, D. M. Kennes, and A. Rubio, Nature Communications **12**, 5644 (2021).
  - <sup>23</sup> L. Wang, E.-M. Shih, A. Ghiotto, L. Xian, D. A. Rhodes, C. Tan, M. Claassen, D. M. Kennes, Y. Bai, B. Kim, *et al.*, arXiv preprint arXiv:1910.12147 (2019).
  - <sup>24</sup> L. Wang, E. M. Shih, A. Ghiotto, L. Xian, D. A. Rhodes, C. Tan, M. Claassen, D. M. Kennes, Y. Bai, B. Kim, K. Watanabe, T. Taniguchi, X. Zhu, J. Hone, A. Rubio, A. N. Pasupathy, and C. R. Dean, Nature Materials **19**, 861 (2020).
  - <sup>25</sup> Z. Zhang, Y. Wang, K. Watanabe, T. Taniguchi, K. Ueno, E. Tutuc, and B. J. LeRoy, Nature Physics **16**, 1093 (2020).
  - <sup>26</sup> E. Li, J.-X. Hu, X. Feng, Z. Zhou, L. An, K. T. Law, N. Wang, and N. Lin, Nature communications **12**, 5601 (2021).
  - <sup>27</sup> T. I. Andersen, G. Scuri, A. Sushko, K. De Greve, J. Sung, Y. Zhou, D. S. Wild, R. J. Gelly, H. Heo, D. Bérubé, *et al.*, Nature Materials **20**, 480 (2021).
  - <sup>28</sup> M. Grzeszczyk, J. Szpakowski, A. Slobodeniuk, T. Kazimierczuk, M. Bhatnagar, T. Taniguchi, K. Watanabe, P. Kossacki, M. Potemski, A. Babiński, *et al.*, Scientific reports **11**, 1 (2021).
  - <sup>29</sup> G. Scuri, T. I. Andersen, Y. Zhou, D. S. Wild, J. Sung, R. J. Gelly, D. Bérubé, H. Heo, L. Shao, A. Y. Joe, *et al.*, Physical Review Letters **124**, 217403 (2020).
  - <sup>30</sup> P. Cudazzo, M. Gatti, and A. Rubio, Physical Review B **86**, 075121 (2012).
  - <sup>31</sup> P. Cudazzo, M. Gatti, and A. Rubio, New Journal of

- Physics **15**, 125005 (2013).
- <sup>32</sup> K. Andersen and K. S. Thygesen, *Physical Review B* **88**, 155128 (2013).
- <sup>33</sup> P. Cudazzo, K. O. Ruotsalainen, C. J. Sahle, A. Al-Zein, H. Berger, E. Navarro-Moratalla, S. Huotari, M. Gatti, and A. , *Physical Review B* **90**, 125125 (2014).
- <sup>34</sup> K. Andersen, K. W. Jacobsen, and K. S. Thygesen, *Physical Review B* **90**, 161410 (2014).
- <sup>35</sup> P. Cudazzo, M. Gatti, and A. Rubio, *Physical Review B* **90**, 205128 (2014).
- <sup>36</sup> Z. Torbatian and R. Asgari, *Journal of Physics: Condensed Matter* **29**, 465701 (2017).
- <sup>37</sup> H. C. Nerl, K. T. Winther, F. S. Hage, K. S. Thygesen, L. Houben, C. Backes, J. N. Coleman, Q. M. Ramasse, and V. Nicolosi, *npj 2D Materials and Applications* **1**, 2 (2017).
- <sup>38</sup> E. Moynihan, S. Rost, E. O'connell, Q. Ramasse, C. Friedrich, and U. Bangert, *Journal of Microscopy* **279**, 256 (2020).
- <sup>39</sup> M. Mazaherifar, M. Elahi, and M. Pourfath, *Journal of Physics D: Applied Physics* **54**, 195304 (2021).
- <sup>40</sup> A. Scholz, T. Stauber, and J. Schliemann, *Physical Review B* **88**, 035135 (2013).
- <sup>41</sup> K. Kechedzhi and D. S. Abergel, *Physical Review B* **89**, 235420 (2014).
- <sup>42</sup> R. E. Groenewald, M. Rösner, G. Schönhoff, S. Haas, and T. O. Wehling, *Physical Review B* **93**, 205145 (2016).
- <sup>43</sup> Y. M. Xiao, W. Xu, F. M. Peeters, and B. Van Duppen, *Physical Review B* **96**, 085405 (2017).
- <sup>44</sup> R. Petersen, T. G. Pedersen, and F. Javier García De Abajo, *Physical Review B* **96**, 205430 (2017).
- <sup>45</sup> J. Van Wezel, R. Schuster, A. König, M. Knupfer, J. Van Den Brink, H. Berger, and B. Büchner, *Physical Review Letters* **107**, 176404 (2011).
- <sup>46</sup> E. Müller, B. Büchner, C. Habenicht, A. König, M. Knupfer, H. Berger, and S. Huotari, *Physical Review B* **94**, 035110 (2016).
- <sup>47</sup> E. Müller, B. Büchner, M. Knupfer, and H. Berger, *Physical Review B* **95**, 075150 (2017).
- <sup>48</sup> W. Zhao, Q. Wu, Q. Hao, J. Wang, M. Li, Y. Zhang, K. Bi, Y. Chen, and Z. Ni, *Applied Physics Letters* **108**, 131903 (2016).
- <sup>49</sup> D. Van Tuan, B. Scharf, I. Zutić, and H. Dery, *Physical Review X* **7**, 041040 (2017).
- <sup>50</sup> B. Scharf, D. Van Tuan, I. Žutić, and H. Dery, *Journal of Physics: Condensed Matter* **31**, 203001 (2019).
- <sup>51</sup> U. Celano and N. MacCaferrri, *Nano Letters* **19**, 7549 (2019).
- <sup>52</sup> F. Karimi, S. Soleimanikahnoj, and I. Knezevic, *Physical Review B* **103**, L161401 (2021).
- <sup>53</sup> S. Venkateswarlu, A. Honecker, and G. Trambly De Laissardière, *Physical Review B* **102**, 81103 (2020).
- <sup>54</sup> G. Giuliani and G. Vignale, *Quantum theory of the electron liquid* (Cambridge university press, 2005).
- <sup>55</sup> S. Yuan, H. De Raedt, and M. I. Katsnelson, *Physical Review B* **82**, 115448 (2010).
- <sup>56</sup> S. Yuan, R. Roldán, and M. I. Katsnelson, *Physical Review B* **84**, 035439 (2011).
- <sup>57</sup> A. Artaud, L. Magaud, T. Le Quang, V. Guisset, P. David, C. Chapelier, and J. Coraux, *Scientific Reports* **6**, 25670 (2016).
- <sup>58</sup> L. Huder, A. Artaud, T. Le Quang, G. T. de Laissardière, A. G. Jansen, G. Lapertot, C. Chapelier, and V. T. Renard, *Physical Review Letters* **120**, 156405 (2018).
- <sup>59</sup> F. Guinea and N. R. Walet, *Physical Review B* **99**, 205134 (2019).
- <sup>60</sup> J.-W. Jiang, *Nanotechnology* **26**, 315706 (2015).
- <sup>61</sup> A. K. Rappe, C. J. Casewit, K. S. Colwell, W. A. Goddard, and W. M. Skiff, *Journal of the American Chemical Society* **114**, 10024 (1992).
- <sup>62</sup> S. Fang, R. Kuate Defo, S. N. Shirodkar, S. Lieu, G. A. Tritsarlis, and E. Kaxiras, *Physical Review B* **92**, 205108 (2015).
- <sup>63</sup> J. C. Slater and G. F. Koster, *Physical Review* **94**, 1498 (1954).
- <sup>64</sup> H. Rostami, R. Roldán, E. Cappelluti, R. Asgari, and F. Guinea, *Physical Review B* **92**, 195402 (2015).
- <sup>65</sup> R. Kubo, *Journal of the Physical Society of Japan* **12**, 570 (1957).
- <sup>66</sup> H. Shi, Z. Zhan, Z. Qi, K. Huang, E. van Veen, J. Á. Silva-Guillén, R. Zhang, P. Li, K. Xie, H. Ji, *et al.*, *Nature Communications* **11**, 371 (2020).
- <sup>67</sup> G. Yu, Z. Wu, Z. Zhan, M. I. Katsnelson, and S. Yuan, *NPJ Computational Materials* **5**, 1 (2019).
- <sup>68</sup> A. Hams and H. De Raedt, *Physical Review E* **62**, 4365 (2000).
- <sup>69</sup> K. Khaliji, T. Stauber, and T. Low, *Physical Review B* **102**, 125408 (2020).
- <sup>70</sup> M. N. Faraggi, A. Arnau, and V. M. Silkin, *Physical Review B* **86**, 035115 (2012).
- <sup>71</sup> A. N. Afanasiev, *arXiv preprint arXiv:2105.05982* (2021).
- <sup>72</sup> T. Stauber, P. San-Jose, and L. Brey, *New Journal of Physics* **15**, 113050 (2013).
- <sup>73</sup> S. Patra, P. Kumari, and P. Mahadevan, *Physical Review B* **102**, 205415 (2020).
- <sup>74</sup> M. Angeli and A. H. MacDonald, *Proceedings of the National Academy of Sciences* **118** (2021).
- <sup>75</sup> M. Mannai and S. Haddad, *Physical Review B* **103**, L201112 (2021).